JNTM JOURNAL of NEW TECHNOLOGY and MATERIALS

Journal of New Technology and Materials

Vol. 15, No. 2 (2025), 24–37

RESEARCH ARTICLE

Temporal Exosome-Gated Immunobioprinting of Collagen/Decellularized Matrix Skin Constructs: A Polarization-Weighted Materials Design Strategy

Umer Shehzad[1,*] and Fatima Zehra[1]

[1]Department of Chemistry, University of Education, Lahore campus, 54000, Pakistan

*Correspondence: umershehzad12@gmail.com

Received date: April 08, 2025; Accepted date: November 27, 2025

Abstract

The key issue that is examined in the present article is whether a bioink for skin can be found using an ordered temporal logic of immune-material behavior. Specifically, TEG-IBP is described as a design approach whereby alginate/gelatin/polydopamine hydrogels are used to set the macrophage status that produces the exosomes, collagen/decellularized ECM (d-ECM) is used to provide the mechanics required for printability, and wound repair metrics assess whether the combination leads to successful integration of immune and other wound-repair processes. Bioink AGP-3, loaded with 0.075 wt% polydopamine nanospheres, showed the highest selectivity index for M2 polarization, $\Psi_{M2} = 1.63$, and thus, was chosen for M2 exosome production. Adding d-ECM to collagen increased the storage modulus to 158854 Pa and low-shear viscosity to 598 mPa s, thereby resulting in a delivery advantage index of 18.5. Multilayer deposition of the epidermal, dermal, vascular, and neural support compartments could be performed at printing speed of 5.5 mm s^{-1} while maintaining filament fidelity in the supporting bath. At 14 days, COL@d-ECM/M2-exosome led to an increase of epidermis thickness from 28.43 ± 3.69 µm in unexposed wounds to 48.58 ± 8.49 µm. In addition, decreased inflammation, enhanced immunoregulation associated with increased CD163 and CD206 content, improved angiogenesis with increased VEGF and CD31 content, and follicle formation were also observed. Thus, a TEG-IBP strategy can indeed result in a material that is better integrated with the host's healing than COL@d-ECM delivery alone. Therefore, the paper presents a JNTM contribution in the form of materials design logic that integrates nano-signaling, immunomodulation with polymers, matrix mechanics, and printing.

Keywords: exosomes, collagen, decellularized extracellular matrix, macrophage polarization, 3D bioprinting, wound healing, immunomodulatory biomaterials, skin regeneration

1 Introduction

In cutaneous wound healing, events such as hemostasis, inflammation, proliferation, matrix deposition, angiogenesis, epithelial resurfacing, and remodeling happen in an orderly fashion over time. Most acute wounds go through all of these processes until complete regeneration occurs. Conversely, chronic, infected, ischemic, diabetic, or other complications will often be trapped in persistent inflammation, excess protease production, increased oxidative stress, poor vascularization, and abnormal matrix turnover. In addition to delayed closure, inflammation impacts the function of fibroblasts, keratinocytes, vascular structures, and increases the likelihood of scar formation. Consequently, modern skin regenerative products must function as dynamic biomaterials capable of modulating immune tone, providing appropriate matrix cues, supporting cell migration, neovascularization, and proper mechanical environment [1–3].

The immune response phase is critical since it connects innate host defense and subsequent regeneration. Early-stage immune response removes pathogens and tissue debris via M1-like macrophages, while the later stage of repair is marked by a transition towards reparative macrophage phenotypes that clear apoptotic cells, reduce inflammation, secrete growth factors, stimulate angiogenesis, and remodel matrix. This is not a binary switch from M1 to M2; macrophages display

a spectrum of phenotypes based on the chemical composition of the surrounding tissue, physical properties, presence of metabolic and tissue damage signals, and the presence of biomaterials with immunomodulatory properties. Nevertheless, increased expression of genes encoding IL-10, TGF-β, CD163, CD206, VEGF, and CSF-1 can still serve as a reliable marker of an anti-inflammatory and reparative microenvironment [4–6]. Importantly, macrophage functions play a crucial role in skin wound repair due to their influence on fibroblasts, vasculature, matrix remodeling, and scar formation [7].

Biomaterials that can modulate macrophages' phenotype are essential tools for wound repair. Macrophage adhesion, mechanical tension in the cytoskeleton, activation of inflammasome, integrin-mediated signaling, and cytokine production are controlled by such properties of materials as matrix stiffness, polymer charge, presence of catechol-based and amine-containing compounds, binding affinity to ligands, rate of degradation, hydration, and nanomechanical properties of the surface. Another way to create immunomodulatory materials is through utilization of a tissue-derived decellularized matrix, which provides collagen, glycosaminoglycan, basement membrane molecules, and biochemical motifs necessary for cell interaction and subsequent remodeling after graft implantation [8–10]. Therefore, material properties can be used as cues in order to direct macrophage polarization before the fabrication of the exosome-containing biomaterial construct.

Extracellular vesicles are a second means to control biomaterials' biological function. As a tool, exosomes allow cells to share bioactive material with distant targets by delivering proteins, lipids, nucleic acids, and signaling mediators, which allows for indirect alteration of the target cell state. In the case of skin wound repair, macrophage-derived vesicles have the potential to control endothelial outgrowth, fibroblast migration, keratinocyte function, inflammatory tone, and matrix remodeling [11]. In addition to their small size, which makes exosomes ideal candidates for hydrogel loading, a successful application of these vesicles in wound repair requires careful consideration of their release profile from a matrix. If the release is too fast, a wound may receive a transient signal from vesicles that will disappear before entering the proliferative phase. Alternatively, slow release may decrease effectiveness of vesicles because of insufficient exposure to the matrix [11–13].

Exosome-loaded hydrogels have shown success in accelerating wound repair by modulating macrophage polarization, supporting angiogenesis, and enhancing bioactive agent persistence [14, 15]. However, one of the major drawbacks is the independent optimization of exosome potency, immunomodulation, matrix stiffness, and construct manufacture, which often leads to incompatible hydrogel and bioinks that are either unable to maintain biological activity, poorly print, or have uneven vesicle distribution. Such challenges become even more important when multiple biological pathways must be activated in a certain order, for instance, keratinocyte function, dermal vascularization, dermal matrix remodeling, and hair follicle-associated remodeling in wound repair.

Three-dimensional printing provides a possibility to precisely control positioning of bioinks loaded with cells, exosomes, and other bioactive agents. Although extrusion printing allows precise patterning of keratinocyte-, fibroblast-, endothelial- and mesenchymal cells, as well as bioactive molecules, such soft hydrogel inks as alginate gel usually have low viscoelasticity, which may lead to filament instability, spreading after extrusion, or deformation before consolidation of polymer network [16, 17]. One solution is printing of hydrogels in a supporting bath, which prevents deformation until the inner hydrogel network strengthens and retains the desired shape [16, 17]. In this context, collagen-based and d-ECM-derived hydrogels are particularly interesting, as collagen represents one of the major components of skin, and d-ECM allows incorporating biological cues obtained from tissue. However, excessive viscoelasticity increases the risk of damaging cells and vesicles inside the bioink, which makes it challenging to find the optimal composition of bioinks [18, 19].

Journal of New Technology and Materials (JNTM) focuses on emerging scientific discoveries and technological advancements in fields such as nanoscience and nanotechnology, including applications in material development. The current work fits into this framework by combining the concept of exosomes, macropahge instructing polymer chemistry, mechanically strong matrix with nanomechanical cues, and bath-assisted extrusion printing into one system.

Temporal exosome-gated immunobioprinting (TEG-IBP) is described as an immune-predominant biomaterial technology for producing exosome-enabled skin constructs. It starts with macrophage polarization, followed by comparison of various alginate/gelatin/polydopamine formulations by their immunomodulatory potential, isolation of most favorable population of vesicles and incorporation of the vesicles into a COL@d-ECM bioink only after immune gating step. Finally, the printed construct is evaluated according to its epidermal thickness, inflammatory marker levels, angiogenic capability, fibrosis score, and ability to induce hair follicle remodeling. The key question in TEG-IBP research is whether temporally ordered immunomodulatory and matrix-gating steps are sufficient to produce a bioink with improved capacity for immunomodulation, neovascularization, and epidermal restoration.

2 Temporal Exosome-Gated Immunobioprinting Methodology

2.1 Design Motivation, Data Source, and Scope of Application

TEG-IBP is designed as a three-level approach to selecting materials for skin regeneration. Level 1 determines the hydrogel that exhibits the best reparative state in terms of inducing the strongest M2-skewing polarization in macrophages. Level 2 confirms that the vesicle-containing matrix has sufficient mechanical properties for bioprinting, elasticity, and exosome presentation. Level 3 checks whether the printed material leads to immune resolution, skin revascularization, dermis

maturation, and epidermis recovery. Variables used for material formulation, macrophage state, rheological measures, printing settings, and wound healing are consistent with the experimental data from Dutta et al.[20]. In this study, these variables are analyzed under the polarization-weighted and delivery-weighted selection criteria to establish direct biological connections between a material and its use in skin regeneration.

TEG-IBP focuses on skin regenerative bioinks as wound recovery is essentially temporal in nature. While the same material may work efficiently at a particular point, its immunological activity, exosome presentation, and mechanical properties are likely to fail at other points of time. Consequently, macrophage training, vesicle selection, and printability have to be considered together in order to ensure proper healing. It means that even the presence of bioactive vesicles alone is not enough to advance a material but requires prior confirmation of the M2-specific macrophage state and the ability to deposit vesicles.

2.2 Material Selection Criteria and Processing Parameters

A total of four formulations of macrophage-instructive matrices were prepared based on alginate and gelatin hydrogels with different contents of polydopamine nanospheres. The concentrations of the matrix were kept at 3% and 2% for alginate and gelatin, respectively. Polydopamine nanospheres were changed within 0-0.075 wt%. The following hydrogels were produced: AG, AGP-1, AGP-2, and AGP-3. RAW 264.7 macrophages were seeded at 4×10^4 cells/well/mL on 10×5 mm^2 printed hydrogels and incubated for 24 hours. All matrices were cross-linked with 100 mM $CaCl_2$ solution after the 24 hour incubation period.

Skin-recovery bioinks contained collagen type I and dermis extracellular matrix extracted from chicken skin. The precursors for COL@d-ECM had 500 mg of d-ECM and 50 mg of collagen. Both ingredients were suspended in acetic acid/pepsin solution and adjusted to pH 7.4. Bioink was printed in a 15% w/v supporting bath made from Pluronic P407, which was gelled at 37 °C. Printing parameters were set as follows: $10 \times 10 \times 5$ mm^3 construct size, 20% infill, 25G nozzle with an inner diameter of 250 µm, printing rate of 5.5 mm s^{-1}, and bed temperature of 37 ± 2 °C. This processing parameter set defines the materials processing space shown in Table 1.

Table 1. Formulation and processing variables used for temporal exosome-gated immunobioprinting, showing how macrophage conditioning, matrix preparation, bath support, and printing geometry are treated as linked material-design decisions rather than isolated experimental settings.

Design block	Specific values	Function in the TEG-IBP strategy
Macrophage-instructive matrix	Alginate 3% (w/v), gelatin 2% (w/v), PDA nanospheres 0, 0.025, 0.05, and 0.075 wt%	Establishes the immune-conditioning material set for selecting the exosome-producing macrophage environment.
Group labels	AG, AGP-1, AGP-2, AGP-3	Provides the ordered material series for calculating macrophage-polarization selectivity.
Macrophage culture condition	RAW 264.7 cells, 4×10^4 cells per well per mL, 24 h culture on 10×5 mm^2 printed hydrogels	Standardizes the early immune-instruction interval.
Hydrogel stabilization	100 mM $CaCl_2$, 24 h hydrogel pre-incubation	Stabilizes alginate/gelatin-based hydrogels before macrophage exposure.
Skin-printing matrix	500 mg d-ECM and 50 mg collagen in acetic acid/pepsin medium; pH adjusted to 7.4	Provides the collagenous and tissue-derived matrix phase for exosome-bearing skin construct fabrication.
Supporting bath	Pluronic P407, 15% (w/v), gelled at 37 °C	Stabilizes soft extruded filaments during multilayer deposition.
Printing configuration	$10 \times 10 \times 5$ mm^3 construct, 20% infill, 25G nozzle, 250 µm inner diameter, 5.5 mm s^{-1} printing speed, 37 ± 2 °C bed temperature	Defines the manufacturable operating point for the COL@d-ECM/M2-exosome construct.

The limits of our methodology are laid out in Table 1. At the same time, the same table ties together chemistry, culture period, matrix processing, stabilization bath, and extrusion shape. This makes sure that the technology is not treated simply as a biological screening technique, and each formulation is evaluated with respect to the ability of producing immune instructive materials that translate into printable wounds-facing constructs.

2.3 Macrophage Polarization Gate for Vesicle-Source Selection

The first selection criterion used the number of M2-associated and M1-associated transcripts found in the respective hydrogel conditioning medium. To determine the polarization selectivity we used Equation 1:

$$\Psi_{M2} = \frac{N_{M2}}{N_{M1} + \varepsilon}. \tag{1}$$

Here N_{M2} and N_{M1} denote the number of M2-associated and M1-associated genes. ε is a constant added only to

prevent division by zero. Since all measured values of N_{M1} are positive, the value of ε does not have any influence on the calculated ration.

Equation 1 transforms macrophage polarization into a decision-making criterion. If the result exceeds unity, the hydrogel induces more reparative genes then inflammatory genes. This gate is intended to guide the material selection process prior to constructing tissue models, but it is not a substitute for a detailed marker-level analysis. Instead, its purpose is to help avoid confusion between a good immune response and an immune response accompanied by inflammatory reaction. Calculated values are summarized in Table 2.

Table 2. Macrophage-polarization values and calculated M2 selectivity used to choose the vesicle-producing condition. The table distinguishes total macrophage activation from repair-biased activation, which is essential for selecting exosomes intended for wound-regenerative signaling.

Hydrogel group	M2-associated genes	M1-associated genes	Ψ_{M2}	Gate decision
AG	118	98	1.20	Passes with modest selectivity
AGP-1	337	214	1.57	Passes with strong selectivity
AGP-2	447	399	1.12	Passes with weak selectivity
AGP-3	473	291	1.63	Selected for vesicle production

The interpretation of Table 2 is that AGP-3 is not selected merely because it produces the largest number of M2-associated transcripts. It is selected because the repair-associated signal remains dominant relative to the inflammatory signal. AGP-2 illustrates why this distinction matters: it has a high M2-associated count, but the simultaneous rise in M1-associated genes lowers its selectivity. The table therefore functions as a decision filter that protects the design from advancing a broadly activating but less repair-biased material.

The largest M2-associated gene count and the highest selectivity index were obtained with AGP-3. Marker-level behavior supported this selection because IL-10 increased by approximately 2-fold, IL-4 and TGF-β exceeded 3-fold, VEGF exceeded 10-fold, and CSF-1 exceeded 3-fold, while NOS2, IL-1β, IL-6, IL-12, and TNF-α were reduced. In the TEG-IBP method, this pattern identifies AGP-3 as the most biologically suitable vesicle-producing condition, not merely as the hydrogel with the largest polydopamine content.

2.4 Structural Delivery Gate for Exosome-Bearing Bioink

After AGP-3 selection, the structural delivery gate was used to determine whether the exosome-bearing matrix satisfied mechanical and delivery requirements for printing. The delivery advantage index was defined as:

$$\Gamma_D = \left(\frac{G'_{COL@dECM}}{G'_{COL}}\right)\left(\frac{\eta_{COL@dECM}}{\eta_{COL}}\right)^{-1}\left(\frac{d_{M2-Exo}}{d_{Ctrl-Exo}}\right), \tag{2}$$

where G' is storage modulus, η is low-shear viscosity, and d is hydrodynamic vesicle diameter.

Equation 2 rewards elastic strengthening, penalizes excessive viscosity increase, and retains vesicle-size behavior as a nanoscale delivery descriptor. This expression is useful because skin bioinks must resist collapse after extrusion while remaining printable under gentle conditions. A high modulus increase without a proportional viscosity penalty indicates that the material can gain shape stability without becoming too resistant to flow. The vesicle-size term is not treated as a stand-alone efficacy predictor; it records that the selected vesicle population differs physically from the control population and may therefore interact differently with the hydrogel network. With $G'_{COL@dECM} = 158854$ Pa, $G'_{COL} = 6240$ Pa, $\eta_{COL@dECM} = 598$ mPa s, $\eta_{COL} = 357$ mPa s, $d_{M2-Exo} = 179$ nm, and $d_{Ctrl-Exo} = 147$ nm, the delivery advantage index is approximately 18.5. This value reflects a large elastic benefit relative to the flow-resistance penalty, which is precisely the materials condition needed for a soft exosome-bearing bioink that must retain geometry after deposition without imposing excessive extrusion burden.

From Table 3, it becomes clear that the design cannot be evaluated according to any specific parameter since the vesicle diameter, fluorescence lifetime, viscosity, storage modulus, epidermis thickness, and fibrosis score reflect different physical and biological aspects at various levels. Therefore, the optimal construct is characterized by the convergence of all of these parameters, where the reinforcement of the matrix enhances residence time, vesicle loading retains the biologically selected scale of information, and the in vivo endpoint confirms that changes in epithelium and immunity are affected by this design but not the ink mechanical properties.

Table 3. Quantitative measurements used for the structural, delivery, and biological gates. These values link nanoscale vesicle characterization, macroscopic matrix mechanics, extrusion-relevant flow behavior, and day-14 wound outcomes in one decision table.

Measurement	Value	Interpretation in TEG-IBP
Control exosome hydrodynamic size	147 ± 2.8 nm	Comparison vesicle population for delivery analysis.
AGP-derived M2-exosome hydrodynamic size	179 ± 1.2 nm	Selected vesicle population associated with AGP-3-guided M2 instruction.
TEM size range	60–140 nm	Confirms nanoscale vesicular morphology compatible with exosome-sized particles.
Low-shear viscosity of COL	357 mPa s	Flow-resistance value for collagen matrix.
Low-shear viscosity of COL@d-ECM	598 mPa s	Increased viscosity that remains compatible with shear-thinning extrusion.
Storage modulus of COL	6240 Pa	Mechanical-stability value for collagen matrix.
Storage modulus of COL@d-ECM	158854 Pa	Stronger elastic network for filament retention and matrix residence.
Native skin elastic modulus	33.8 ± 2.5 kPa	Tissue-level mechanical comparator.
d-ECM elastic modulus	18.7 ± 1.9 kPa	Softer fibrous matrix after decellularization.
Remaining DNA in d-ECM	approximately 0.8%	Indicates effective decellularization and reduced cellular residue.
Exosome fluorescence lifetime	17.6 ± 0.6 ns for pure exosome; 12.8 ± 0.4 ns for hydrogel-encapsulated exosome	Indicates optical persistence after hydrogel loading, with shorter lifetime after matrix interaction.
Epidermal thickness at day 14	Control: 28.43 ± 3.69 µm; COL@d-ECM: 30.36 ± 6.14 µm; COL@d-ECM + Exo: 48.58 ± 8.49 µm	Histological outcome for epidermal restoration.
Fibrosis score	Control: 1; COL@d-ECM and COL@d-ECM + Exo: 2	Indicates moderate collagen deposition in hydrogel-treated wounds.

2.5 Construct Fabrication and Regenerative Readout Categories

According to the selected COL@d-ECM/M2-exosome bioink, the construct represents a model skin, including epidermal, dermal, vascular, and neural compartments. The presence of human keratinocytes was considered a sign of the epidermal layer, while the presence of human dermal fibroblasts was the indication of a dermal matrix. Human mesenchymal stem cells were responsible for vascular and neural compartments. Bioink was deposited in a Pluronic bath and transferred to the culture medium. The key point of methodology consists of the sequence of conditions, whereby the type of vesicles (macrophage polarization), their suitability for delivery (rheological properties), and positioning of the ink (bioprinting conditions) were established.

The four regenerative processes include immune resolution, angiogenesis, epithelial differentiation, and matrix remodeling. The immune resolution was evaluated according to M1/M2 shifts, inflammatory genes' behavior, suppression of CD86/NOS2-related activities, and promotion of CD163/CD206 activities. Angiogenesis was evaluated based on VEGF, CD31, endothelial tubes, and sprouting abilities. Epithelial differentiation was analyzed using keratin family proteins, keratinocyte maturation, and epidermis thickness. Fibronectin, collagen-related genes, Masson's trichrome staining, and fibrosis scoring served as a basis for matrix remodeling. All quantitative data are presented as means ± standard deviations, where statistical significance refers to $p < 0.05$, $p < 0.01$, and $p < 0.001$.

3 Reparative Performance and Mechanistic Interpretation

Among the formulations analyzed using the polarization gate, AGP-3 was determined to be the best macrophage-conditioning hydrogel, based on $\Psi_{M2} = 1.63$. This result means that AGP-3 produced the greatest ratio of reparative to inflammatory gene features with respect to other conditions, such as AG, AGP-1, and AGP-2. This outcome makes biological sense, since the chemical nature of the nanospheres (polydopamine) enables interactions involving catecholamines in the hydrogel-cell interface, leading to greater macrophage adhesion and mechanotransduction of signals associated with inflammatory resolution and reparative gene expression. It is also aligned with the notion that the material chemistry may actively control macrophage responses, rather than just avoid triggering their inflammatory phenotypes [21, 22].

The genetic pattern supports this conclusion, with increases in the number of M2 markers, such as IL-4, IL-10, TGF-β, VEGF, and CSF-1, and decreases in the number of M1 markers, such as NOS2, IL-1β, IL-6, IL-12, and TNF-α. This indicates that AGP-3 is capable of generating a M2 phenotype suitable for promoting the process of inflammation resolution and angiogenesis. Wound repair involves coordination between multiple cell types (macrophages, fibroblasts, endothelial cells, and keratinocytes), therefore the formulation selection should be based on the induction of a stable reparative macrophage phenotype. Vesicles formed from incomplete cells cannot serve the purpose effectively.

AGP-1 also possessed a strong ability to induce the M2 phenotype ($\Psi_{M2} = 1.57$), while AGP-3 provided the highest number of M2-associated genes, as well as the highest selectivity index. However, AGP-2 demonstrated the highest increase in the number of genes involved in some categories of transcripts; its selectivity value was equal to 1.12, which was due to simultaneous increase in M1-associated gene transcripts. Thus, the proposed selection criterion allows avoiding the mistake of choosing a bioactive material with respect to total gene expression level only. Selection based on this parameter may be misleading because it does not account for immunoregulatory activity. The index provides a solution to this problem,

allowing advancement of AGP-3 to vesicle preparation, as demonstrated in Figure 1.

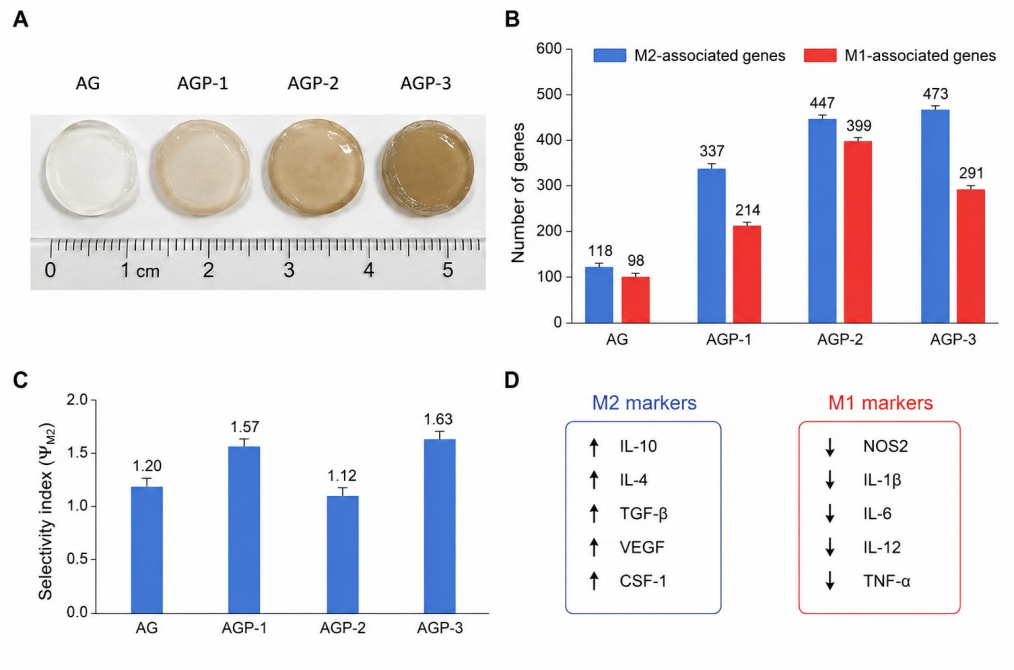

Figure 1. AGP hydrogel screening and macrophage-polarization gate. (A) Macroscopic appearance of alginate/gelatin and alginate/gelatin/polydopamine hydrogels with increasing polydopamine nanosphere content. (B) Comparative M2- and M1-associated gene counts for the screened hydrogel groups. (C) Calculated M2 selectivity index used for the TEG-IBP immune-selection gate. (D) Marker-level direction showing enrichment of reparative macrophage signals and reduction of inflammatory markers. AGP-3 provides the strongest reparative bias and is therefore selected as the vesicle-producing condition.

The data provided in Figure 1 offer the first empirical proof that the immune instruction of macrophages is formulation-dependent and that an increase in polydopamine content does not generate a simple and naive ”the more the better” trend. AGP-3 formulation is significant in the context of this research since it is characterized by enrichment of the reparative marker set without proportional elevation of the inflammatory one. Therefore, the figure proves the existence of immune gate necessary to use AGP-3-conditioned macrophages as a source for exosomes incorporation into a printed construct.

The AGP-derived M2-exosome population was found to have a hydrodynamic diameter of 179±1.2 nm, whereas vesicles produced by unconditioned macrophages had the diameter of 147 ± 2.8 nm. Both populations preserve the characteristic vesicle nanomorphology, and the 60-140 nm size range observed in TEM images supports this conclusion. A relatively high diameter of the M2-exosome population might be due to differences in the surface proteins, the hydration shell, aggregation or bio-molecular cargo of vesicles. From a hydrogel perspective, such a parameter matters because size and surface composition of vesicles affect their interaction with the matrix, diffusivity, ability to come into contact with cells, and uptake (Figure 2).

Nevertheless, biological significance of a vesicle population is far more critical than its physical characteristics. Since vesicles used in this study originate from macrophages subjected to conditioning with the AGP-3 hydrogel, they carry the ’history’ of immune instruction, meaning their selection depends on the status of their parent cells. The main advantage of such vesicle selection strategy in comparison to the exosome loading approach is that a vesicle population may enter the skin construct only if its parent cells are already in repair-polarization. The rationale behind this approach is the need for an effective transition between inflammatory resolution and vascular-epithelial stages of skin wound healing. VEGF and CD31 expression patterns and endothelial associated responses confirm the angiogenic nature of the selected exosome population.

It means that the exosome-loaded construct is capable of supporting vascular activation and not only pro-inflammatory immune response, and tube formation and sprouting reactions are additional proof. Such a finding is vital from the biological point of view because efficient epidermal restoration needs a well-vascularized wound bed. Oxygen and nutrient supply provided by angiogenesis is crucial for the paracrine stimulation of collagen deposition and keratinocyte migration in addition to other aspects of wound healing [23, 24].

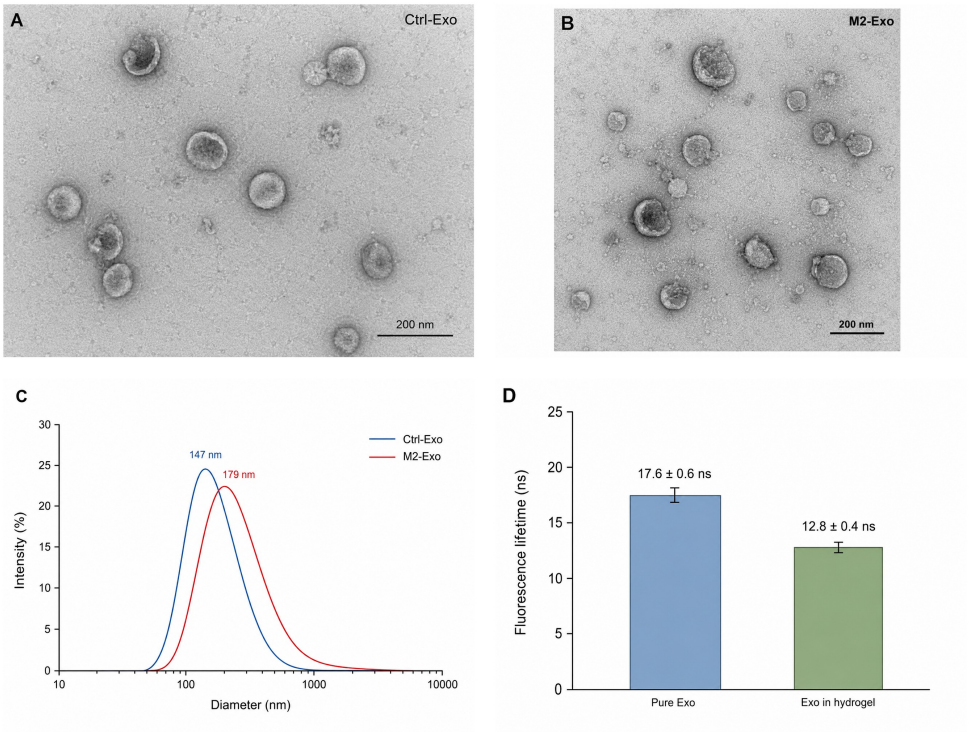

Figure 2. Morphological, size, and fluorescence-lifetime characterization of the exosome populations. (A,B) Transmission electron microscopy images of control macrophage exosomes and AGP-conditioned M2 exosomes, showing nanoscale vesicular morphology. (C) Size-distribution comparison indicating a shift from the control vesicle population toward the larger M2-exosome hydrodynamic diameter. (D) Fluorescence-lifetime measurement for pure exosomes and hydrogel-encapsulated exosomes, confirming optical persistence after matrix loading with a shorter lifetime after encapsulation.

Figure 2 confirms that the chosen vesicle population is still within the nanoscale range suitable for paracrine therapy based on hydrogels while simultaneously having a difference from the control group of macrophages. Shorter fluorescence lifetime upon encapsulation into the matrix does not disqualify the delivery mechanism, as it simply implies changes in optical and molecular microenvironment. Therefore, the figure provides a link between the biological gate and the delivery process: vesicles conditioned by AGP can be transported using the matrix, maintaining exosome-related signals.

In turn, the structural gate confirmed the positive materials balance provided by COL@d-ECM. Low-shear viscosity increased by 1.67x – from 357 to 598 mPa s when moving from collagen only to COL@d-ECM. Even more impressively, the storage modulus went up 25.46x – from 6240 to 158854 Pa. Hence, the elasticity enhancement factor was larger by orders of magnitude compared to the viscosity price, allowing one to conclude that the new matrix would be easier to print. Such results have importance for extrusion bioprinting since the printed material needs sufficient cohesion to maintain filament integrity; however, large viscosity change can lead to an increased shear stress that may negatively impact cell viability and precision of printing. Thus, COL@d-ECM increases elasticity while retaining relatively moderate viscosity levels.

First of all, decellularized ECM provided valuable mechanical properties, with the elastic modulus being equal to 18.7 ± 1.9 kPa, making the material softer compared to native skin (33.8 ± 2.5 kPa). Furthermore, the remaining DNA concentration was around 0.8%, showing that decellularization was successful. It allows one to consider d-ECM as a potential skin-related matrix component due to its ability to provide fibrous tissue-like environment while reducing the effect of donor cells presence. Recent studies on decellularized matrices and bioinks revealed that tissue-derived matrices retain some of the properties characteristic of their tissue of origin, facilitating cell adhesion, differentiation, and even remodeling [19, 25, 26].

A delivery advantage index of approximately 18.5 suggests that the proposed COL@d-ECM/M2-exosome system gained much more in elastic stability compared to its viscosity cost while transporting the chosen vesicle population. This value cannot be treated as any measure of therapeutical value. Instead, it is an indicative of the ratio of elasticity to viscosity gain while delivering therapeutic compounds. The matrix is relatively rigid but hydrated enough to support cells; besides, it is biologically recognizable due to collagen and decellularized nature. Overall, in JNTM terms, we demonstrated the effectiveness of one materials design approach, where nanoscale therapeutic vesicles are delivered by a tuned bioink, as illustrated by Figure 3.

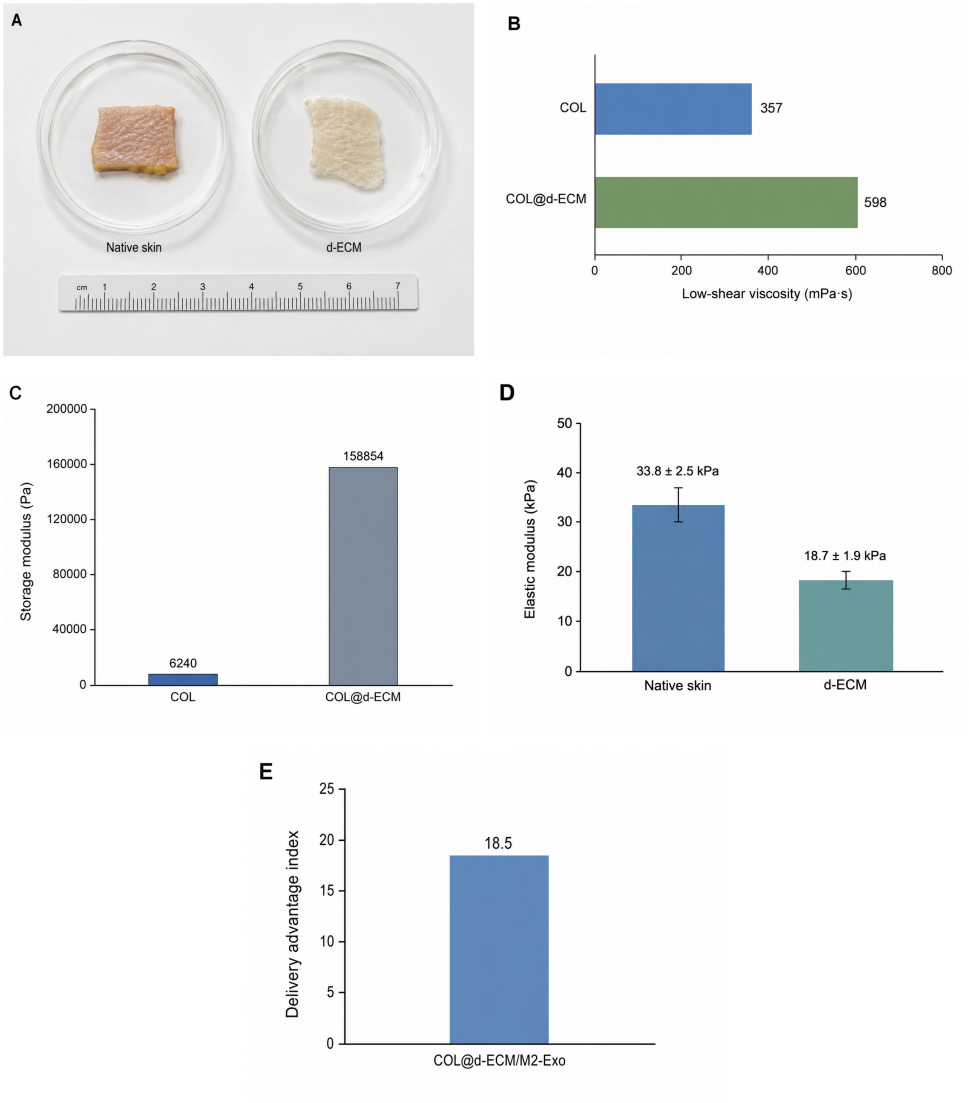

Figure 3. Decellularized skin matrix preparation and structural delivery gate for COL@d-ECM/M2-exosome bioink. (A) Gross appearance of native skin and the decellularized extracellular matrix. (B) Low-shear viscosity comparison showing the moderate flow-resistance increase after d-ECM incorporation. (C) Storage-modulus comparison showing the strong elastic reinforcement of COL@d-ECM relative to collagen alone. (D) Elastic modulus comparison between native skin and d-ECM. (E) Delivery advantage index indicating that the elastic gain outweighs the viscosity penalty while preserving the selected M2-exosome delivery function.

Figure 3 explains why COL@d-ECM is the appropriate carrier for the selected vesicles. The mechanical gain is large enough to improve post-extrusion residence, but the viscosity increase remains moderate. This means that d-ECM functions as more than a biological additive: it also restructures the collagen network into a mechanically more competent carrier. The figure therefore supports the second gate of the TEG-IBP sequence, where delivery suitability is judged by both matrix mechanics and vesicle compatibility.

The selected printing speed of 5.5 mm s^{-1} falls within the stable filament-fidelity window of approximately 5–6 mm s^{-1}. Speeds below this range produced overly thick filaments, whereas higher speeds, especially beyond 10 mm s^{-1}, produced excessively thin or unstable filaments. This behavior is consistent with soft shear-thinning bioinks, where filament diameter is governed by extrusion rate, nozzle motion, bath resistance, matrix recovery, and interfacial stability. A stable filament is not merely a cosmetic printing outcome; it determines the distribution of cells, exosomes, and matrix architecture throughout the construct.

The supporting Pluronic bath plays a key role in maintaining the printed geometry before the COL@d-ECM network stabilizes. Bath-assisted printing is particularly useful for low-modulus or slowly consolidating hydrogels because the bath provides temporary support during deposition. In the present design, the bath enables multilayer organization without forcing the bioink to become so viscous that extrusion would damage cells or disrupt vesicle integrity. The selected speed therefore represents a compromise between spatial fidelity and biological gentleness. This compromise is central to the TEG-IBP method because a biologically potent exosome population cannot function predictably if printing disperses it

unevenly or damages the cellular components of the construct.

A materials-based interpretation is needed here. Printability is often treated as a fabrication parameter, but in exosome-bearing bioinks it is also a delivery parameter. Uneven filaments can create local exosome-rich and exosome-poor regions, altering immune and angiogenic signaling across the wound interface. Excessive shear may also influence cell viability and vesicle distribution. The stable filament window therefore acts as the point at which matrix mechanics, manufacturing control, and biological dosing intersect. By placing printability after macrophage and structural gates, TEG-IBP ensures that the chosen operating condition is biologically meaningful rather than arbitrarily selected, as shown in Figure 4.

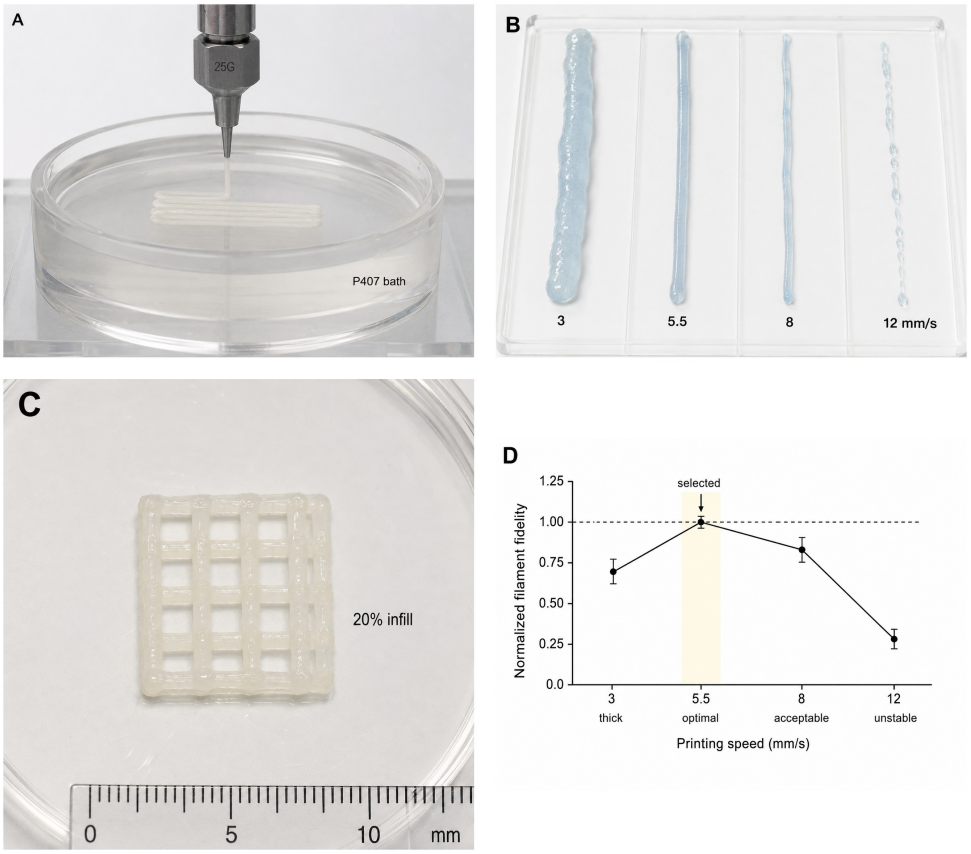

Figure 4. Supporting-bath printing and filament-fidelity optimization. (A) Extrusion of COL@d-ECM/M2-exosome bioink into the Pluronic P407 supporting bath. (B) Printed filaments obtained at representative translation speeds, demonstrating thick deposition at low speed and unstable thinning at high speed. (C) Multilayer grid construct printed at the selected 20% infill condition. (D) Normalized filament-fidelity profile identifying approximately 5.5 mm s^{-1} as the stable operating point for the exosome-bearing construct.

Figure 4 illustrates that the manufacturing parameters themselves play a role in therapeutic design, as opposed to being a separate technical consideration. Slow printing results in material deposition that forms thick filaments, whereas fast printing reduces deposition stability, thinning out the material layer. The optimized operating point avoids both scenarios to deposit material that allows a more even distribution of exosomes and cells. Figure 4 thus provides the manufacturing gate that makes it possible to implement biological design in a three-dimensional skin construct.

The multi-layered construct was designed with skin compartments in mind, wherein keratinocytes were placed in the epidermal layer, fibroblasts provided the dermal matrix, and mesenchymal stem cells participated in vascular and neuronal compartments. The cell viability was high during the entire week of cultivation, demonstrating the absence of cytotoxic conditions in the printing process and/or matrix composition. More importantly, the addition of exosomes into the co-culture promoted skin-specific signals of maturation. There was an increase in fibronectin and COL1A1 expression levels, implying that the skin matrix was being developed. There was an increase in KRT1, KRT5, and KRT14 expressions associated with epidermal differentiation.

Transcriptomic enrichment provides additional evidence for maturation behavior. The enriched epidermis program involved several gene families such as late cornified envelope and keratin family genes, as well as IGFBP5, ALOX3, CDSN, SCEL, TGM1, GATA6, and LGR5. Genes and pathways involved are compatible with epidermal development, keratinocyte differentiation, growth factor binding, scaffold interaction, and collagen maturation. It should be noted that the objective here was not the production of fully matured tissue within seven days of in vitro cultivation, which would be

incorrect and misleading to interpret the results in this way. Instead, the transcriptome indicated the movement toward skin-like maturation driven by matrix cues and exosome signaling.

These observations illustrate why d-ECM and exosomes should be considered together. COL@d-ECM serves as a matrix, providing the physical architecture and tissue-released molecules, whereas M2 exosomes serve as an inflammatory regulator, delivering paracrine signals. The behavior of fibroblasts is thus influenced by both the physical and biochemical characteristics of the construct. Keratinocytes are developing in an environment where inflammation and angiogenesis are being regulated. Such coupling is consistent with the modern paradigm in engineering of skin substitutes, where the coordination of multiple components (vascular, epithelial, immune, etc.) is critical to success [17, 27]. The TEG-IBP framework offers a feasible way to approach the problem by providing a hierarchy of design.

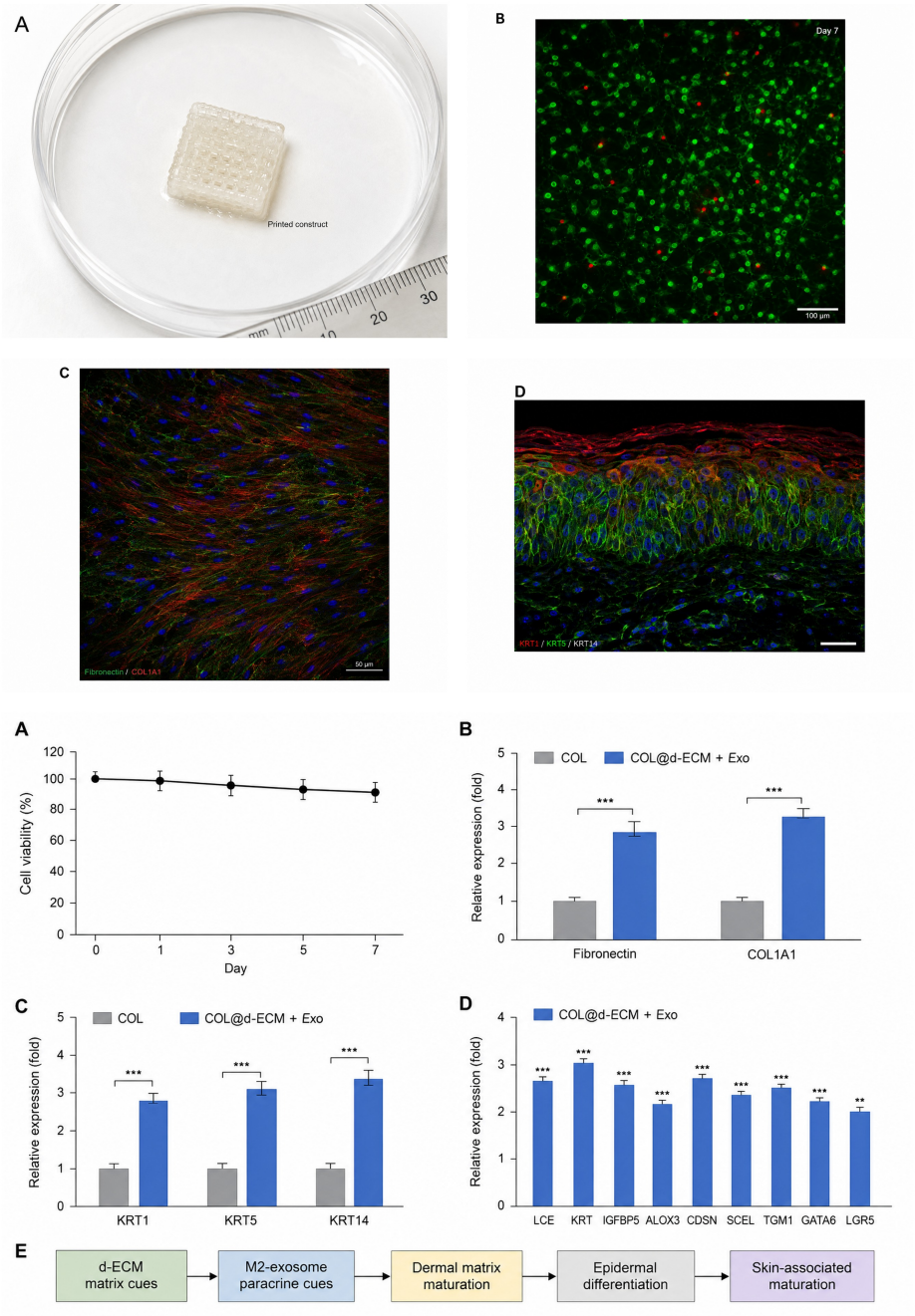

Figure 5. Printed construct architecture and in vitro skin-associated maturation. (A) COL@d-ECM/M2-exosome construct after supporting-bath printing. (B) Live/dead staining showing favorable cell survival after seven days of culture. (C) Cytoskeletal organization within the construct, indicating cell spreading and matrix interaction. (D) Epidermal marker staining showing stratification-associated organization in the printed construct. (E) Quantitative and longitudinal readouts for viability, dermal matrix markers, keratinocyte markers, and construct maturation, supporting the interpretation that the d-ECM/M2-exosome environment drives skin-associated cellular behavior rather than serving only as a passive carrier.

Figure 5 demonstrates that the construct cannot be considered as an inert carrier of cells and nanovesicles. Indications such as viability, cytoskeletal spreading, epidermal markers distribution, and expression of extracellular matrix-related genes demonstrate active interaction of the cells with the printed scaffold. Therefore, it is reasonable to consider the obtained result as maturation towards epithelial arrangement and not as a tissue replacement effect. Such an approach can be more accurate, since the in vitro analysis demonstrated directional changes in maturation, but not in differentiation.

Day 14 measurement of wound repair addresses the main research question. The results show that epidermal thickening occurred in the group exposed to the exosome-bearing group, when compared to the control condition. While control animals demonstrated epidermal thickness of 28.43 ± 3.69 µm, the COL@d-ECM-alone group demonstrated the thickening of 30.36 ± 6.14 µm, and the COL@d-ECM/M2-exosome condition exhibited thickness of 48.58 ± 8.49 µm. In comparison with the control condition, the increase of the thickness was 70.9%, and in comparison with COL@d-ECM alone, the enhancement was equal to 60.0%. The minimal increase for the COL@d-ECM-alone condition suggests that only matrix delivery did not ensure the expected response. On the other hand, the strong enhancement in the exosome-bearing condition proves that signaling performed by the M2-exosome provided an essential biological effect beyond matrix delivery, see Figure 6.

Immune reaction was altered according to expectations. In the exosome-bearing case, inflammatory scoring was decreased, and the reduction of IL-6 and TNF-α expression occurred on the wound bed. Moreover, immunostaining showed that the inflammatory reaction with participation of CD86/NOS2 became less pronounced, while reparatory reaction with the presence of CD163/CD206 became enhanced. Such results are essential because they show closure of the TEG-IBP logic chain: the selected vesicle population ensured the formation of immune-resolving wound interface. As such, the materials' choice predicted the biological outcome, and not just described it.

Furthermore, the angiogenic response complemented the epithelial reconstruction response. The increased production of VEGF protein and CD31 expression demonstrated vascularization in the wound site, while KRT-family genes' activity and epidermis thickening indicated epithelial reconstruction. In addition to biological plausibility of the effect, these two outcomes are biologically connected: vascularization ensures the improved metabolic state for the regenerating tissue, while the absence of inflammatory burden allows the organization of fibroblasts and migration of keratinocytes. Overall, TEG-IBP can be considered as materials design improvement.

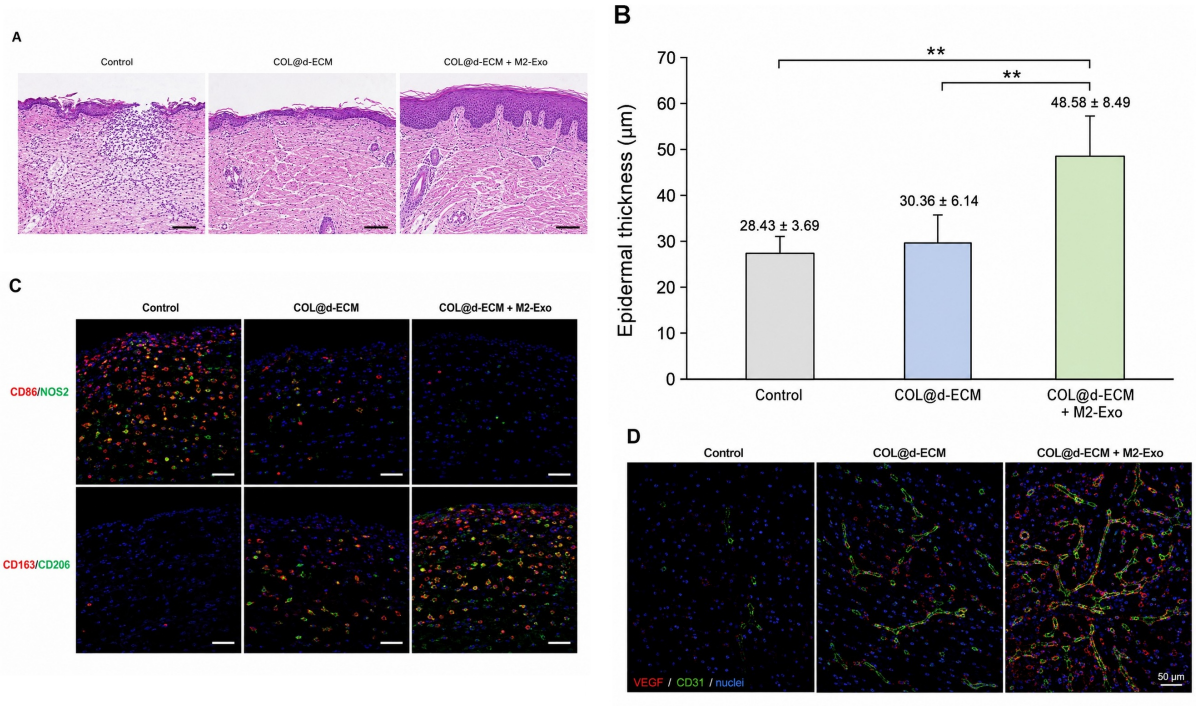

Figure 6. Day-14 epithelial restoration, macrophage phenotype, and angiogenic response in the wound bed. (A) Hematoxylin-and-eosin histology comparing control, COL@d-ECM, and COL@d-ECM/M2-exosome conditions. (B) Epidermal-thickness quantification showing the strongest epithelial restoration in the COL@d-ECM/M2-exosome group. (C) Immunostaining of CD86/NOS2 and CD163/CD206 showing reduced inflammatory activity and strengthened reparative macrophage-associated response. (D) VEGF/CD31 staining showing enhanced angiogenic support in the exosome-bearing construct.

Figure 6 represents the most decisive test of the paper's research question, namely that the matrix-alone group produces minimal change in epidermal thickness in comparison with untreated wounds, while the exosome group produces a large increase in thickness alongside an immunangiogenic shift. The figure thus clearly illustrates that the presence of matrix

alone is not sufficient; an appropriate M2-exosome signal is required to enable the bioprinted matrix to act as an effective biological repair scaffold.

Matrix remodeling proved to be somewhat more complicated. The control group had partial granulation tissue, while the COL@d-ECM and COL@d-ECM/M2-exosome groups were characterized by moderate collagen deposition with fibrosis score of 2. This finding requires careful consideration since while collagen deposition is important for proper dermal regeneration, excessive collagen buildup can result in fibrosis. The moderate fibrosis score shows that the presented construct promotes matrix formation, while simultaneously calling for further optimization, namely, regulation of exosome concentration, duration of their retention in the matrix, and matrix degradation itself. In this way, the TEG-IBP approach is beneficial, as it does not treat wound healing as merely an increase in wound closure rate, but also emphasizes other important criteria, such as matrix deposition regulation, immune resolution, and epithelial reconstitution.

The finding of more advanced hair-follicle associated tissue remodeling adds further information about the biologically active construct. The COL@d-ECM/M2-exosome condition was found to induce gene signatures associated with KRT14, KRT15, KRT17, SOX9, COL-IV, FBN1, and SMAD3. These markers are linked with activity of epithelial progenitors, keratinocyte activation, basement membrane remodeling, fibrillar matrix organization, and growth factor-induced tissue reformation. Time-dependent single-cell analysis indicated decreased inflammatory cell types and increased M2-associated activities, which is consistent with the idea of appendage-associated remodeling driven by a combination of epithelial, mesenchymal, vascular, and immune interactions. Hair follicle regeneration is a demanding biological endpoint, and therefore, the current endpoint should be treated as hair follicle-associated remodeling and not appendage formation, as illustrated in Figure 7.

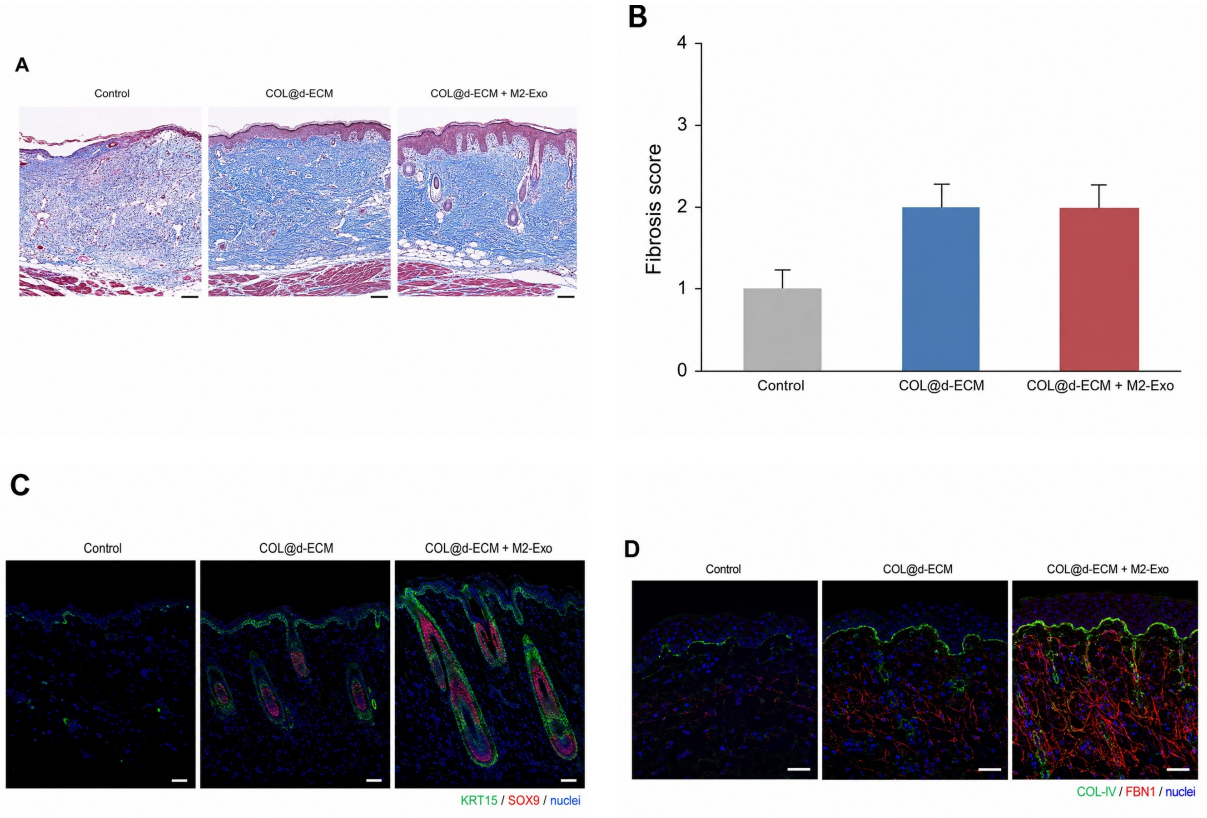

Figure 7. Matrix remodeling and hair-follicle-associated repair endpoints. (A) Masson's trichrome staining for collagen deposition. (B) Fibrosis scoring revealing moderate collagen deposition in the hydrogel-treated conditions. (C) KRT5/SOX9 staining for epithelial appendages and markers. (D) COL-IV/FN1 staining for basal membrane and matrix remodeling markers. The combination of endpoints shows hair follicle-associated remodeling, but also indicates a need to regulate collagen deposition.

Figure 7 adds another layer of complexity to the positive results obtained. While the exosome-containing construct improved appendage-associated and basal membrane remodeling, the fibrosis score reveals that collagen deposition requires additional regulation. This figure demonstrates that the results are balanced since while TEG-IBP facilitates coordinated repair, the next step of its improvement must necessarily include regulation of excessive collagen deposition to avoid undesirable fibrosis.

In conclusion, the integrated mechanism underlying the presented results can be described as follows. AGP-3 selects the population of M2-enriched and angiogenic macrophages, which are then loaded onto a COL@d-ECM matrix that acts as an elastic support for further printing and tissue engineering. Bath-assisted printing maintains the geometric structure

of the matrix and distributes cells and vesicles evenly in a multilayer scaffold. Implantation of the scaffold produces a wound interface characterized by less inflammation, greater activity of M2-associated immune cells, better angiogenesis, increase in epidermal thickness, and hair follicle remodeling.

The presented results fully answer the research question, demonstrating that a temporally ordered design based on selection of M2-enriched and angiogenic macrophages and a COL@d-ECM matrix enables identification of bioprintable skin constructs superior to matrix delivery only in terms of skin healing. The strongest evidence is provided by AGP-3 with the highest degree of M2-selective activity, COL@d-ECM, allowing for significant elastic properties with no excessive increase in viscosity, an appropriate printing speed resulting in good filament shape preservation, and the exosome-bearing construct increasing epidermal thickness while shifting inflammation and angiogenesis markers toward desirable values. The problem left for future research is regulation of exosome dose, their release period, and degradation of the matrix itself.

One should note that the key benefit of the presented method is the shift in the decision-making process for skin bioprinting: instead of selecting a matrix, delivering vesicles, performing printing, and analyzing wound healing, the method involves a selection of immune phenotypes prior to exosome production and mechanical assessment prior to implantation. This approach decreases the possibility that an interesting vesicle population is matched with an improper matrix, or vice versa. The practical significance of this study is also linked to the development of a new material methodology applicable to screening of new vesicle sources, matrices, and printing windows with the help of the same gate sequencing.

4 Conclusion

The current study investigated whether an exosome-loaded skin construct could be selected in a temporally-ordered design route and whether such a selection would lead to greater coherence in wound healing compared with COL@d-ECM delivery only. Both questions are positively answered through the ability of TEG-IBP to link M2-polarization with matrix mechanics and filament fidelity in a single decision sequence. Specifically, AGP-3 was selected based on a strong healing bias, where $\Psi_{M2} = 1.63$, meaning that exosomes targeted for regenerative delivery must be chosen not only with regards to their composition but also with regards to the biological properties of the cell line that produced them. Then, COL@d-ECM provided a structurally sound carrier for the vesicles, allowing the storage modulus of the mixture to be increased from 6240 to 158854 Pa without a strong increase in low-shear viscosity (357 vs 598 mPa s). The delivery advantage index of 18.5 and the stable printability of 5.5 $\mathrm{mm\,s^{-1}}$ prove that biological properties of vesicles, structural integrity of a matrix and printability of the construct must be considered jointly. From the biological perspective, COL@d-ECM/M2-exosome delivery significantly improved the day-14 wound healing with an increase of epidermis thickness to 48.58 ± 8.49 μm, in comparison with 28.43 ± 3.69 μm and 30.36 ± 6.14 μm in untreated wounds and COL@d-ECM only, respectively, thus proving the ineffectiveness of matrix delivery alone. In addition, the exosome-laden construct decreased inflammation, stimulated CD163/CD206-mediated immune modulation, promoted VEGF/CD31-based angiogenesis and follicular remodeling. The above findings confirm the importance of the M2-gated exosome signal in converting a simple printable d-ECM matrix into a more bioactive construct. The major limitation of the method consists in its inability to completely prevent fibrosis caused by the gel treatment. Future studies should further fine-tune the doses, release time, matrix composition, mechanical properties, and structure of the constructs and explore exosomes' influence using prolonged wound-healing assessment, dose-response analysis, release profile measurement, and mechanical testing of the healed tissue. Under these conditions, the TEG-IBP approach allows for obtaining an interesting JNTM-oriented materials platform, which is built on the integration of exosome biology, macrophage instructive polymer chemistry, mechanics of a decellularized matrix and extrusion-based bioprinting technology.

References

[1] A. J. Singer and R. A. F. Clark, Cutaneous wound healing, *New England Journal of Medicine* 341 (1999) 738–746.

[2] G. C. Gurtner, S. Werner, Y. Barrandon, and M. T. Longaker, Wound repair and regeneration, *Nature* 453 (2008) 314–321.

[3] S. A. Eming, P. Martin, and M. Tomic-Canic, Wound repair and regeneration: mechanisms, signaling, and translation, *Science Translational Medicine* 6 (2014) 265sr6.

[4] M. L. Novak and T. J. Koh, Macrophage phenotypes during tissue repair, *Journal of Leukocyte Biology* 93 (2013) 875–881.

[5] P. J. Murray, J. E. Allen, S. K. Biswas, E. A. Fisher, D. W. Gilroy, S. Goerdt, S. Gordon, J. A. Hamilton, L. B. Ivashkiv, T. Lawrence, M. Locati, A. Mantovani, F. O. Martinez, J.-L. Mege, D. M. Mosser, G. Natoli, J. P. Saeij, J. L. Schultze, K. A. Shirey, A. Sica, J. Suttles, I. Udalova, J. A. van Ginderachter, S. N. Vogel, and T. A. Wynn, Macrophage activation and polarization: nomenclature and experimental guidelines, *Immunity* 41 (2014) 14–20.

[6] N. X. Landen, D. Li, and M. Stahle, Transition from inflammation to proliferation: a critical step during wound healing, *Cellular and Molecular Life Sciences* 73 (2016) 3861–3885.

[7] T. A. Wynn and K. M. Vannella, Macrophages in tissue repair, regeneration, and fibrosis, *Immunity* 44 (2016) 450–462.

[8] H. Lee, S. M. Dellatore, W. M. Miller, and P. B. Messersmith, Mussel-inspired surface chemistry for multifunctional coatings, *Science* 318 (2007) 426–430.

[9] D. Seliktar, Designing cell-compatible hydrogels for biomedical applications, *Science* 336 (2012) 1124–1128.

[10] J. Li, X. Jiang, H. Li, M. Gelinsky, and Z. Gu, Tailoring materials for modulation of macrophage fate, *Advanced Materials* 33 (2021) 2004172.

[11] C. Thery, K. W. Witwer, E. Aikawa, M. J. Alcaraz, J. D. Anderson, R. Andriantsitohaina, A. Antoniou, T. Arab, F. Archer, G. K. Atkin-Smith, and others, Minimal information for studies of extracellular vesicles 2018 (MISEV2018), *Journal of Extracellular Vesicles* 7 (2018) 1535750.

[12] M. Colombo, G. Raposo, and C. Thery, Biogenesis, secretion, and intercellular interactions of exosomes and other extracellular vesicles, *Annual Review of Cell and Developmental Biology* 30 (2014) 255–289.

[13] R. Kalluri and V. S. LeBleu, The biology, function, and biomedical applications of exosomes, *Science* 367 (2020) eaau6977.

[14] K. Wang, R. Dong, J. Tang, H. Li, J. Dang, Z. Zhang, and others, Exosomes laden self-healing injectable hydrogel enhances diabetic wound healing via regulating macrophage polarization to accelerate angiogenesis, *Chemical Engineering Journal* 430 (2022) 132664.

[15] P. Liu, Y. Xiong, L. Chen, C. Lin, Y. Yang, Z. Lin, and others, Angiogenesis-based diabetic skin reconstruction through multifunctional hydrogel with sustained releasing of M2 macrophage-derived exosome, *Chemical Engineering Journal* 431 (2022) 132413.

[16] T. J. Hinton, Q. Jallerat, R. N. Palchesko, J. H. Park, M. S. Grodzicki, H.-J. Shue, M. H. Ramadan, A. R. Hudson, and A. W. Feinberg, Three-dimensional printing of complex biological structures by freeform reversible embedding of suspended hydrogels, *Science Advances* 1 (2015) e1500758.

[17] M. Hospodiuk, M. Dey, D. Sosnoski, and I. T. Ozbolat, The bioink: a comprehensive review on bioprintable materials, *Biotechnology Advances* 35 (2017) 217–239.

[18] F. J. O'Brien, Biomaterials and scaffolds for tissue engineering, *Materials Today* 14 (2011) 88–95.

[19] F. Pati, J. Jang, D.-H. Ha, S. W. Kim, J.-W. Rhie, J.-H. Shim, D.-H. Kim, and D.-W. Cho, Printing three-dimensional tissue analogues with decellularized extracellular matrix bioink, *Nature Communications* 5 (2014) 3935.

[20] S. D. Dutta, J. M. An, J. Hexiu, A. Randhawa, K. Ganguly, T. V. Patil, T. Thambi, J. Kim, Y.-K. Lee, and K.-T. Lim, 3D bioprinting of engineered exosomes secreted from M2-polarized macrophages through immunomodulatory biomaterial promotes in vivo wound healing and angiogenesis, *Bioactive Materials* 45 (2025) 345–362, doi:10.1016/j.bioactmat.2024.11.026.

[21] B. N. Brown, R. Londono, S. Tottey, L. Zhang, K. A. Kukla, M. T. Wolf, K. A. Daly, J. E. Reing, and S. F. Badylak, Macrophage phenotype as a predictor of constructive remodeling following the implantation of biologically derived surgical mesh materials, *Biomaterials* 33 (2012) 3792–3802.

[22] K. Sadtler, A. Singh, M. T. Wolf, X. K. Wang, D. M. Pardoll, and J. H. Elisseeff, Design, clinical translation and immunological response of biomaterials in regenerative medicine, *Nature Reviews Materials* 1 (2016) 16040.

[23] M. Potente, H. Gerhardt, and P. Carmeliet, Basic and therapeutic aspects of angiogenesis, *Cell* 146 (2011) 873–887.

[24] J. Rouwkema and A. Khademhosseini, Vascularization and angiogenesis in tissue engineering: beyond creating static networks, *Trends in Biotechnology* 34 (2016) 733–745.

[25] S. F. Badylak, D. O. Freytes, and T. W. Gilbert, Extracellular matrix as a biological scaffold material: structure and function, *Acta Biomaterialia* 5 (2009) 1–13.

[26] B. S. Kim, H. Kim, G. Gao, J. Jang, and D.-W. Cho, Decellularized extracellular matrix: a step towards the next generation source for bioink manufacturing, *Biofabrication* 9 (2017) 034104.

[27] S. V. Murphy and A. Atala, 3D bioprinting of tissues and organs, *Nature Biotechnology* 32 (2014) 773–785.